

## Controllable Growth of Vertically Aligned Aluminum-Doped Zinc Oxide Nanorod Arrays by Sonicated Sol–Gel Immersion Method depending on Precursor Solution Volumes

Mohamad Hafiz Mamat<sup>1\*</sup>, Zuraida Khusaimi<sup>2</sup>, Musa Mohamed Zahidi<sup>1</sup>, Suriani Abu Bakar<sup>2</sup>, Yosri Mohd Siran<sup>3</sup>, Syahril Anuar Md Rejab<sup>3</sup>, Ahmad Jaril Asis<sup>3</sup>, Shawaluddin Tahiruddin<sup>3</sup>, Saifollah Abdullah<sup>2</sup>, and Mohamad Rusop Mahmood<sup>1,2\*</sup>

<sup>1</sup>NANO-ElecTronic Centre (NET), Faculty of Electrical Engineering, Universiti Teknologi MARA (UiTM), 40450 Shah Alam, Selangor, Malaysia

<sup>2</sup>NANO-SciTech Centre (NST), Institute of Science (IOS), Universiti Teknologi MARA (UiTM), 40450 Shah Alam, Selangor, Malaysia

<sup>3</sup>Sime Darby Research Sdn Bhd, Pulau Carey, Klang, Selangor, Malaysia

Received November 27, 2010; accepted January 4, 2011; published online June 20, 2011

Aluminium (Al)-doped zinc-oxide (ZnO) nanorod arrays have been successfully prepared using a novel and low-temperature sonicated sol–gel immersion method. The photoluminescence (PL) spectrum reveals the appearance of two emission peaks from the nanorod that are centred at 381 and 590 nm. The nanorod has a hexagonal structure with a flat-end facet, as observed using field-emission electron microscopy (FESEM). Interestingly, all samples have similar surface morphologies and diameter sizes of 40 to 150 nm after immersion in different precursor-solution volumes. The thickness-measurement results show that the thicknesses of the samples increase after immersion in higher precursor-solution volumes. We show for the first time that the growth of nanorod arrays along the *c*-axis can be controlled using different precursor volumes, and its growth mechanism is discussed. X-ray diffraction (XRD) spectra indicate that the prepared nanorods are ZnO with a hexagonal wurtzite structure that grows preferentially along the *c*-axis. © 2011 The Japan Society of Applied Physics

### 1. Introduction

Zinc oxide (ZnO) nanostructures have been extensively studied due to their potential applications in nanodevices such as sensors,<sup>1</sup> solar cells,<sup>2</sup> and light-emitting devices.<sup>3</sup> ZnO is a II–VI group semiconductor material with a wide band-gap energy of 3.3 eV and a high exciton binding energy of 60 meV. It is an environmentally friendly and non-toxic material that has superior physical and chemical properties, including radiation hardness, thermal stability and biocompatibility.<sup>4,5</sup>

Recently, many efforts have been made to synthesise one-dimensional (1D) ZnO nanostructures, especially vertically aligned nanorod or nanowire arrays, due to their attractive characteristics for various applications. These nanostructures have large surface areas with high aspect ratios, quantum confinement and high electron mobility compared to nanoparticle thin films which exhibit an electron-trapping phenomenon within grain boundaries. Many techniques have been used to produce vertically aligned ZnO nanorod or nanowire arrays, including pulsed laser deposition,<sup>6</sup> electrochemical deposition,<sup>7</sup> vapor–liquid–solid (VLS) growth,<sup>8</sup> and hydrothermal deposition or solution immersion.<sup>9</sup> Solution immersion is especially attractive because of its low-cost, low-temperature synthesis, and the simplicity of its experimental setup. Furthermore, the controllable growth of nanorods is achievable under a solution immersion method by optimising the solution and deposition parameters. The controllable growth of aligned ZnO nanorods is very important for achieving the desired level of functionality and for satisfying application requirements. Many researchers have reported on controlling the growth of aligned ZnO nanorods by changing solution concentration and prolonging immersion time.<sup>10,11</sup> In this paper, we highlight the effects of the volume of the precursor-solution on the controllable growth of aligned aluminium (Al)-doped ZnO nanorods along the *c*-axis using a novel low-temperature method involving sonicated sol–gel immersion. We doped the ZnO nanorod with Al because Al-doped ZnO nanostructures are

regarded as potential semiconductor materials in device fabrication, which yields high conductivity without deterioration in optical transmittance and crystallinity.<sup>12,13</sup> To the best of our knowledge, there has been no report on the growth behaviour of vertically aligned ZnO nanorods at different precursor volumes.

### 2. Experimental Procedure

In our experiment, Al-doped ZnO nanorod arrays were grown on a seed-layer-coated glass substrate using a sonicated sol–gel immersion method.<sup>14</sup> The seed layer, which consists of Al-doped ZnO nanoparticles, was deposited on the glass substrates by sol–gel spin coating. The details on the seed-layer preparation are described elsewhere.<sup>15</sup> Al-doped ZnO nanorod arrays were grown using aqueous solutions of 0.1 M zinc nitrate hexahydrate [Zn(NO<sub>3</sub>)<sub>2</sub>·6H<sub>2</sub>O; 98% purity; System], 0.1 M hexamethylenetetramine (HMT; H<sub>2</sub>NCH<sub>2</sub>CH<sub>2</sub>OH; 99% purity; Aldrich), and 0.001 M aluminium nitrate nonahydrate [Al(NO<sub>3</sub>)<sub>3</sub>·9H<sub>2</sub>O; 98% purity; Analar]. The use of zinc nitrate rather than zinc acetate makes the nucleation of ZnO nanostructures more feasible because precipitation occurs more easily in solutions containing nitrate salt.<sup>16</sup> The reagents were dissolved and reacted in a beaker filled with distilled water as a solvent under ultrasonic irradiation at 50 °C for 30 min with an ultrasonic water bath (Hwasin Technology Powersonic 405, 40 kHz). Next, the solution was stirred and aged for 3 h at room temperature.

The resulting solution was poured into vessels with different volume capacities of 50, 100, 250, 500, and 1000 ml. The seed-layer-coated-glass substrates were placed at the bottom of each vessel. Next, the sealed vessels were transferred into a water bath instrument for the hydrothermal process. During this process, the temperature was maintained at 95 °C. After 4 h of immersion, the vessels were removed from the hot water bath, and the samples were immediately removed from the vessels. The nanostructures deposited on the substrates were rinsed with distilled water and dried in a furnace at 150 °C for 10 min.

The photoluminescence (PL) properties of the synthesised nanorods were investigated using a PL spectrophotometer

\*E-mail address: hafiz\_030@yahoo.com

with a helium–cadmium (He–Cd) excitation laser at 325 nm (Horiba Jobin Yvon-79 DU420A-OE-325). The surface and cross-sectional images of Al-doped ZnO nanorod arrays were observed by a field-emission scanning electron microscopy (FESEM; ZEISS Supra 40VP). The compositional analysis of the prepared nanorods was characterised using electron-dispersive X-ray spectroscopy (EDX; INCA) with FESEM. The thicknesses of the samples were measured using a surface profiler (KLA Tencor P-6). The crystalline phase and crystallite orientation were characterised using X-ray diffraction (XRD; Rigaku Ultima IV).

### 3. Results and Discussion

Figure 1 depicts the PL spectrum of aligned Al-doped ZnO nanorod prepared using 100 ml precursor solution, which was measured at room temperature. The nanorod has two types of emission peaks, which are located in the ultraviolet (UV) band region (381 nm) and the visible (vis) region (590 nm). The UV emission peak corresponds to the near-band-edge transitions of ZnO due to the recombination of free excitons, and the peak position is close to the ZnO band-gap energy (3.3 eV).<sup>17</sup> The wide and strong visible emission peak is widely attributed to defect states in ZnO.<sup>18,19</sup> It is obvious from the PL spectrum that the visible emission intensity is more dominant than the UV emission in our nanorod sample. This finding indicates that the synthesised nanorods in this deposition process are rich in atomic defects.<sup>20,21</sup> Similar PL characteristics have also been reported in other studies.<sup>17,22</sup>

There are a few techniques that could be considered for defect passivation on the ZnO-nanorod surface. For instance, Lin *et al.* reported that using H<sub>2</sub>-plasma treatment, the PL properties were improved by a factor of 60 for the relative intensity ratio (i.e., UV emission to deep-level emission).<sup>23</sup> It has also been reported that treatment in O<sub>2</sub> plasma removes defects such as OH groups on the ZnO surface.<sup>24,25</sup> Besides plasma treatment, the annealing process in ambient or gaseous ambient (i.e., O<sub>2</sub>, H<sub>2</sub>, N<sub>2</sub>, etc.) conditions is also useful to reduce the defect concentration in nanorods.<sup>26,27</sup> This annealing treatment could quench the visible emission by desorbing OH groups from the nanorod surface, thereby reducing the dislocation, point defects, and other irradiative recombination centres that are related to the surface/interface state. These measures will be applied to our nanorods in the future to reduce the incidence of defect.

Figure 2 shows FESEM images that provide plane and cross-sectional views of the prepared Al-doped ZnO nanorod arrays grown on seed-layer-coated glass substrates. From the images, it is clear that large-scale, well-oriented Al-doped ZnO nanorods were deposited on the substrates in uniform and dense arrays. The nanorods have a hexagonal shape structure with flat-top facets. The size of the nanorod diameters in the sample prepared using 50 ml of precursor [Fig. 2(a)] range from 40 to 150 nm. Further increasing the precursor volume to 250, 500, and 1000 ml, the diameters of the nanorods remain almost unchanged, as observed in Figs. 2(b), 2(c), and 2(d). However, the cross-sectional images of the nanorods prepared using 50 and 1000 ml of precursor solution, as shown in Figs. 2(e) and 2(f), respectively, reveal that the lengths of the nanorods differ between the two samples and increase after exposure to

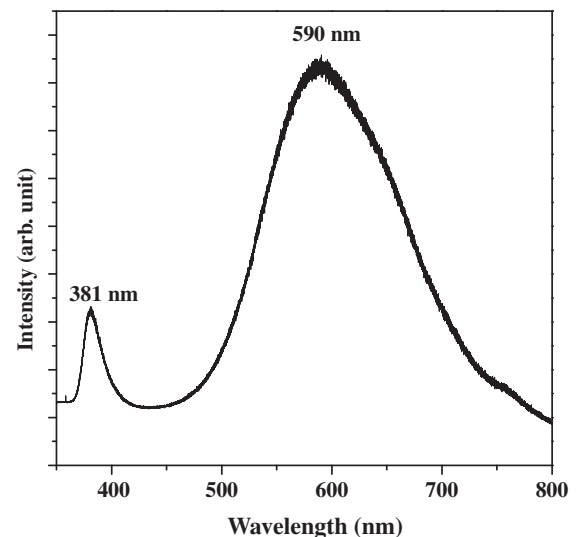
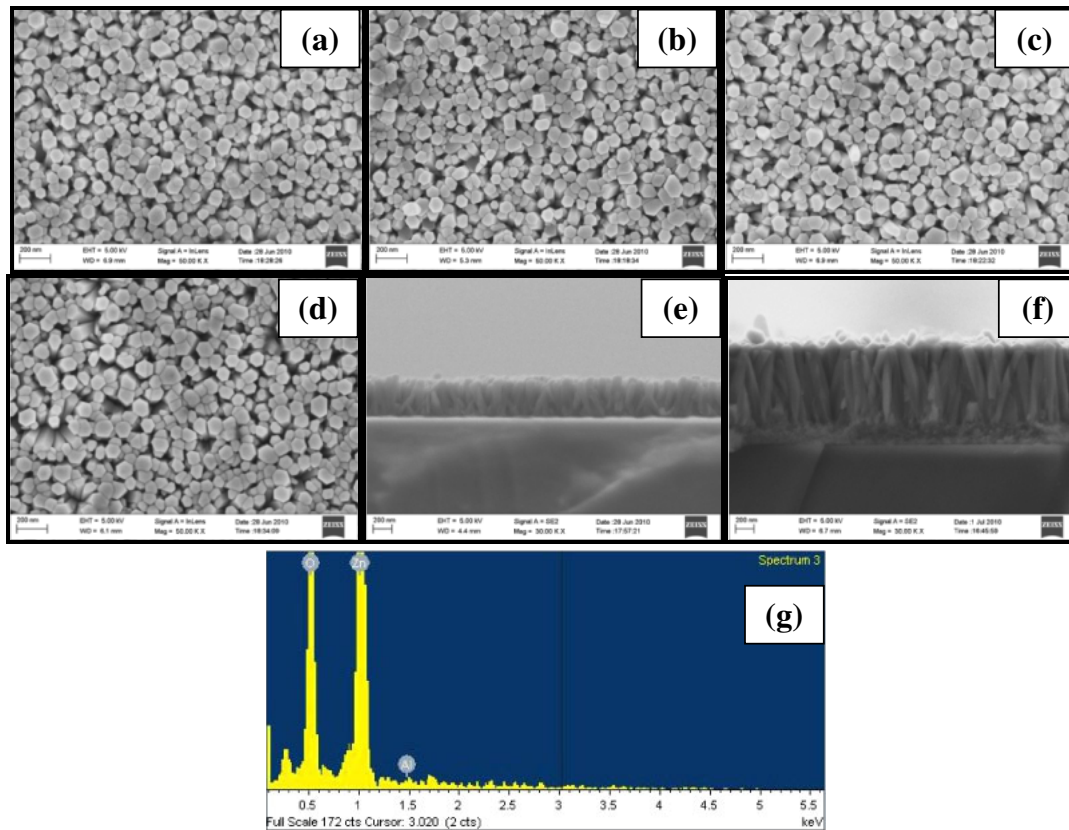


Fig. 1. PL spectrum of a synthesised aligned Al-doped ZnO nanorod array.

higher precursor-solution volumes. The EDX measurement results, as shown in Fig. 2(g), confirm the existence of Al in the nanorod with an atomic ratio of Al : Zn : O = 1 : 39 : 60.

To investigate growth behaviour, we conducted thickness measurements to characterise the length of the nanorods grown with different precursor-solution volumes. Figure 3 shows the thickness measurements of the nanorod arrays prepared with different precursor-solution volumes. Note that the seed layer used for this experiment has an average thickness of 186 nm. After the immersing the seed-layer-coated glass substrate into 50 ml of precursor solution, the thickness of the film increased to 438 nm. When 100 ml of precursor solution was used, the thickness of the sample improved to 674 nm. This trend of increasing sample thickness is also shown after immersion into 250, 500, and 1000 ml of precursor solution, resulting in average thickness values of 754, 891, and 1320 nm, respectively. From this result, we concluded that nanorod growth behaviour using our process occurs primarily along the *c*-axis when the immersion process is carried out using relatively high precursor volumes. It is interesting to note that the nanorod dimension increases in length only when immersed in relatively high volumes of precursor-solution, without significantly affecting the size of the nanorod diameter. This result indicates that the controllable growth of the nanorods along the *c*-axis can be achieved under different volumes of precursor-solution using our sonicated sol–gel immersion method.

The crystal structure of the aligned Al-doped ZnO nanorod arrays were characterised using XRD measurements. Figure 4 shows the XRD patterns of Al-doped ZnO nanorod arrays prepared with different precursor volumes and a seed layer. All nanorod samples show diffraction peaks, which can be indexed as the hexagonal phase of ZnO with a wurtzite structure (JCPDS 36-1451). The XRD peaks of the seed layer are relatively weak compared to the prepared nanorods. Figure 4 shows that the (002)-plane-orientation peak centred at 34.4° is the strongest peak, giving the highest intensity compared to the other peaks. The results



**Fig. 2.** (Color online) FESEM images of Al-doped ZnO nanorod arrays prepared using (a) 50, (b) 250, (c) 500, and (d) 1000 ml precursor solution. Cross-sectional images of nanorod arrays prepared using (e) 50 and (f) 1000 ml precursor solution. (g) EDX pattern of the Al-doped ZnO nanorod array.

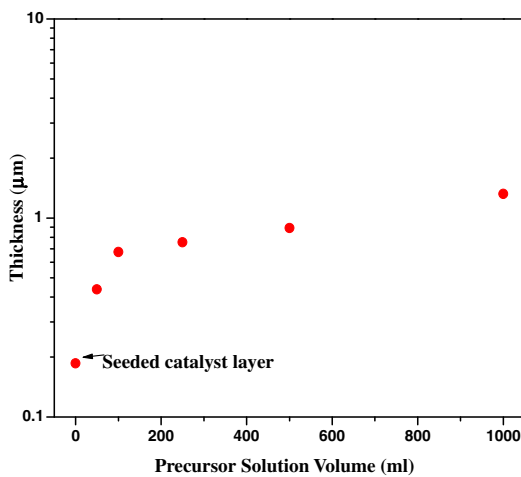


**Fig. 3.** (Color online) Plots of Al-doped ZnO array thickness (with 186 nm seeded catalyst layer) versus precursor volume.

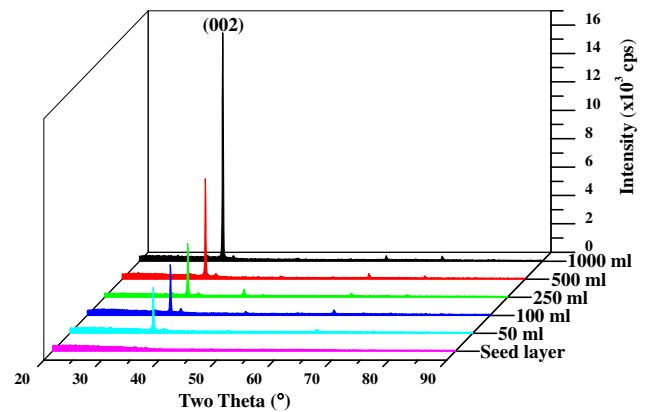
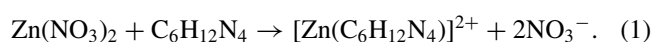


**Fig. 4.** (Color online) XRD spectra of aligned Al-doped ZnO nanorod arrays prepared using different volumes of precursor-solution.

indicate that nanorod growth occurs preferentially along the *c*-axis or perpendicular to the substrate. Other orientation peaks with very weak intensities in the XRD spectra might be due to imperfect nanorod alignment on the substrate.<sup>28)</sup> The intensity of the (002) peak improves when the nanorods are grown using as the precursor volume increases. This result suggests that nanorod growth is more active at higher precursor volumes, which produce longer nanorods on the seed-layer-coated glass substrate.

Based on these results, we can predict a possible growth mechanism for the formation of well-aligned ZnO nanorod

arrays on the seed-layer-coated glass substrate using the sonicated sol-gel method. We suspect that the controllable growth along the *c*-axis might be caused by the effects of the sonication process on the precursor solution, which disperse and mix the zinc nitrate (i.e., the precursor) and the HMT (i.e., the stabiliser) very well. The sonication process also helps crush the agglomerated zinc nitrate and HMT particles, which hasten physical- and chemical-reaction activity in the solution. This process enables the  $Zn^{2+}$  ion to react effectively with the HMT, as shown by<sup>29)</sup>



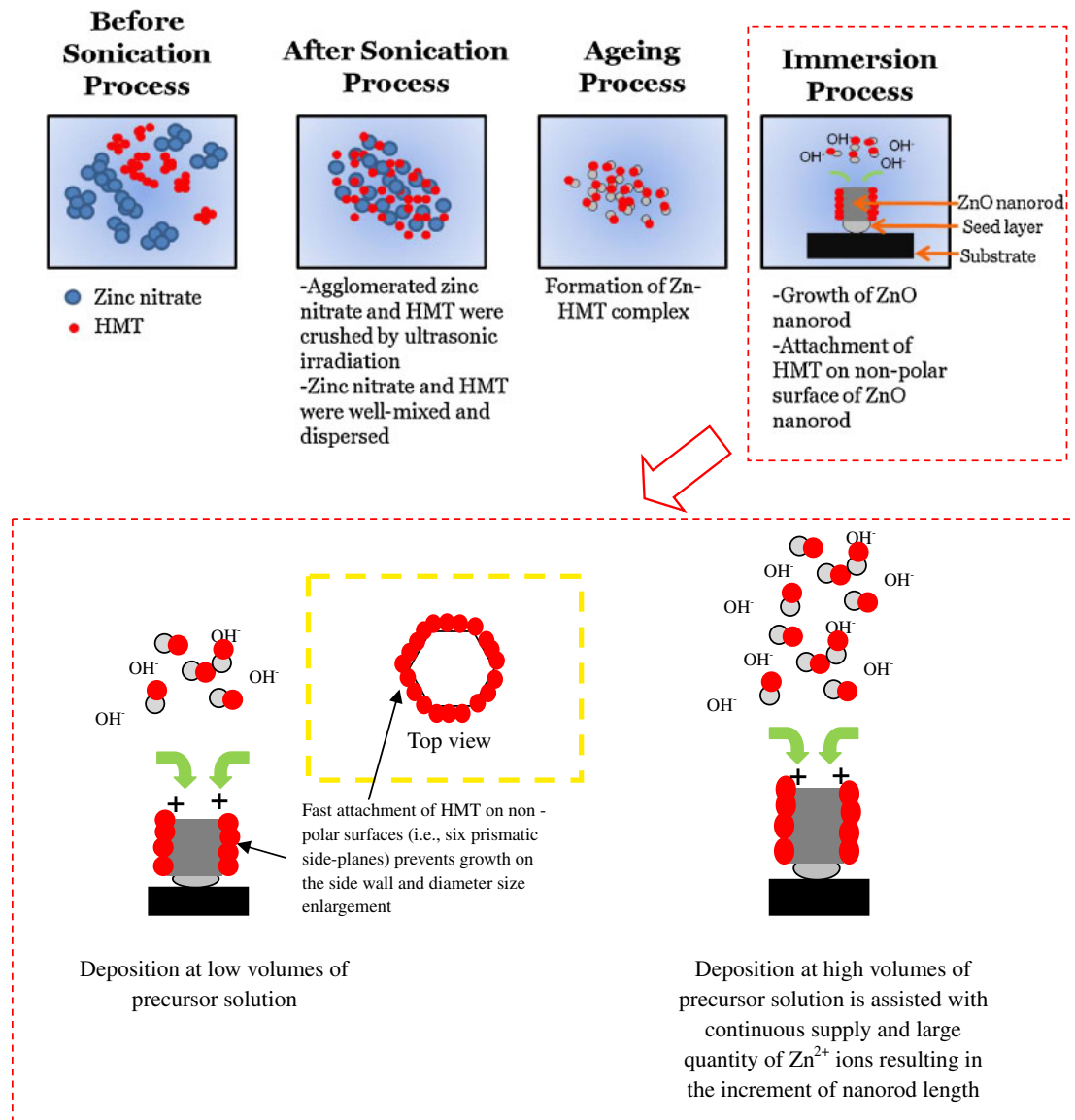
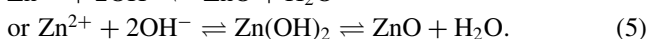
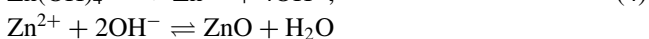
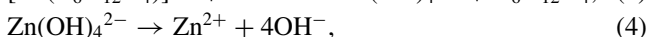
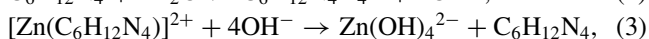


Fig. 5. (Color online) A possible growth mechanism of aligned nanorod arrays using the sonicated sol-gel immersion method.

The HMT plays a very important role in controlling the growth of the aligned ZnO nanorods. When it attaches to the Zn<sup>2+</sup> ions, particle agglomeration is reduced, and the formation of ZnO in the solution is slowed.

During the hydrothermal process, the seed catalyst layer provides a base that initiates the growth of nanorod arrays through heterogeneous nucleation. It is generally accepted that heterogeneous nucleation on a seed-layer surface occurs more easily than homogenous nucleation.<sup>30</sup> The seed layer provides the lowest energy barrier for heterogeneous nucleation, which produces almost negligible lattice mismatch between the nanorods.<sup>8,31</sup> This condition results in the growth of high-quality aligned nanorod arrays on the substrates. The general reactions occurring during the hydrothermal process can be described by<sup>29,32</sup>



Initially, when the Zn<sup>2+</sup> ion and OH<sup>-</sup> exceed supersaturation, ZnO nuclei form on the seed-layer surface, initiating the growth of aligned ZnO nanorods. It has been suggested that the HMT also acts as a non-polar chelating agent that attaches to the non-polar facets of ZnO nanorods.<sup>33</sup> Because of this attachment behaviour, epitaxial growth along the *c*-axis is facilitated because only the (0001) plane is exposed during the growth process. Because the growth rate in the (0001) direction is the fastest in the hydrothermal system,<sup>34,35</sup> the ZnO nanorods grow preferentially in the (0001) direction, which is vertically aligned with the substrate. Based on the experimental results, the growth rate of the nanorod on the substrate along the *c*-axis is faster when higher precursor volumes are used. This condition might be due to the continuous supply of Zn<sup>2+</sup> ions on the top of the nanorods, which is more available in higher precursor volumes. The heterogeneous growth of ZnO becomes dominant when Zn<sup>2+</sup> ions exist in large quantities due to the equilibrium condition in eq. (5), which moves to the right and thus results in nanorod growth. Thus, nanorod formation along the *c*-axis using higher precursor

volumes is faster because of the equilibrium kinetics in the solution. Because the pH of the solution in this study is 6.2 before the reaction and 5.6 after the immersion process for all volumes, which is much lower than the isoelectric point of ZnO (8–10) under both conditions,<sup>36)</sup> the nanorods are positively charged (i.e., Zn<sup>2+</sup>-terminated surface) and attract negatively charged species in the solution. As a result, nanorod growth is sped up in the preferred *c*-axis direction.

Good dispersion and mixing processes between the precursor and the stabiliser through sonication might help control the diameter size of the nanorod because the HMT can immediately attach onto the non-polar facets (i.e., six prismatic side-planes) after the ZnO nanorod nucleation process on the seed layer. The HMT acts as a buffer layer at non-polar surfaces, which disturbs ZnO deposition on these surfaces. This condition disables rapid growth on the side walls or the non-polar surface of the nanorod, which maintains an almost constant diameter size. The fast attachment of the HMT onto the ZnO surface prevents nanorod growth in the direction of non-polar facets, thus hindering an enlargement in nanorod diameter. Because the ZnO nanorods were confined by the HMT molecules on their non-polar surfaces and had only the polar surface for further growth, directional growth along the *c*-axis was achieved at different precursor volumes with an almost constant diameter. The possible growth mechanism of the nanorod arrays is illustrated in Fig. 5.

Previously, under the hydrothermal deposition technique, nanorod growth behaviour has been reported to vary in terms of dimension (i.e., both diameter and length) if one of the deposition or solution parameters are changed. For instance, Guo *et al.* reported that both the axial and radial growth rates were increased after deposition for longer periods in the hydrothermal system.<sup>30)</sup> Similarly, Niarchos *et al.* reported diameter- and length-dependence of nanorods on precursor-solution molarity during the hydrothermal process, in which sizes increased at higher precursor molarities.<sup>37)</sup> These trends showing lateral and vertical nanorod enlargement are also reported by other groups after immersion time and precursor concentration were increased using the hydrothermal method.<sup>38–41)</sup> The report suggests that controllable growth along the *c*-axis under the hydrothermal method is difficult and requires the optimisation of both the precursor molar concentration and immersion time, which must be changed simultaneously. However, there are a few techniques that have been reported as showing axial-growth behaviour with minimal increment or controllable growth of the diameter size. For example, Guo *et al.* have demonstrated nanorod growth along the *c*-axis with small increases in diameter by nanoparticle-assisted pulsed-laser deposition (NAPLD).<sup>6)</sup> Their method enables the control of the density of the nanorods deposited onto substrates. A finding by Hirate *et al.* is also promising and quite interesting.<sup>42)</sup> They reported the controllable growth of ZnO nanorod diameters using chemical-vapor deposition (CVD) combined with laser ablation using a multi-step deposition. By controlling the oxygen flow rate in their system, they increased nanorod length while achieving a diameter that was either the same, smaller, or larger than the initial nanorod.

#### 4. Conclusions

In conclusion, using a sonicated sol–gel immersion deposition method, we have successfully prepared Al-doped ZnO nanorod arrays oriented along the *c*-axis with controllable lengths by varying precursor volumes. The use of a seed layer induced the anisotropic growth of ZnO nanorods on the substrate with good crystallinity. The PL spectrum reveals that the synthesised nanorod array has strong visible emission at 590 nm and weak UV emission at 381 nm. It is observed through surface morphology images that the size of the diameter is almost constant for all samples, and it ranges 40 to 150 nm after immersion in different precursor volumes. However, the cross-sectional images and thickness results indicate that the sample thickness increased with the volume of the precursor-solution. The XRD results show that all nanorod arrays prepared at different precursor volumes have preferential growth along the (002) plane, which is vertical or perpendicular to the substrates. The stronger intensity peak behaviour of the (002) plane after immersion in higher precursor volumes suggests an improvement in the crystallinity of the nanorod. This condition also indicates that nanorod growth has been strengthened, thereby leading to increases in samples thicknesses at higher precursor volumes.

#### Acknowledgements

One of the authors (Mohamad Hafiz Mamat) would like to thank Universiti Teknologi MARA (UiTM) Malaysia and Jabatan Perkhidmatan Awam (JPA) Malaysia for their financial support. The authors also would like to thank the Faculty of Applied Sciences (Mr. Hayub) and Faculty of Mechanical Engineering, UiTM for FESEM and XRD facilities, respectively. The author thanks Mr. Suhaimi Ahmad (UiTM technician), Mrs. Nurul Wahida (UiTM Asst. Science Officer) and Mr. Mohd Azlan Jaafar (UiTM technician) for their kind support of this research.

- 1) N. Koshizaki and T. Oyama: *Sens. Actuators B* **66** (2000) 119.
- 2) M. Ichimura and H. Takagi: *Jpn. J. Appl. Phys.* **47** (2008) 7845.
- 3) H. Yamauchi, Y. Watanabe, M. Iizuka, M. Nakamura, and K. Kudo: *Jpn. J. Appl. Phys.* **48** (2009) 04C167.
- 4) T. Ma, M. Guo, M. Zhang, Y. Zhang, and X. Wang: *Nanotechnology* **18** (2007) 035605.
- 5) Ü. Özgür, Y. I. Alivov, C. Liu, A. Teke, M. A. Reshchikov, S. Dogan, V. Avrutin, S. J. Cho, and H. Morkoc: *J. Appl. Phys.* **98** (2005) 041301.
- 6) R. Guo, J. Nishimura, M. Matsumoto, M. Higashihata, D. Nakamura, and T. Okada: *Jpn. J. Appl. Phys.* **47** (2008) 741.
- 7) O. Lupan, V. M. Guerin, I. M. Tiginyanu, V. V. Ursaki, L. Chow, H. Heinrich, and T. Pauporte: *J. Photochem. Photobiol. A* **211** (2010) 65.
- 8) P. K. Giri, S. Dhara, and R. Chakraborty: *Mater. Chem. Phys.* **122** (2010) 18.
- 9) L. Vayssieres, K. Keis, S. E. Lindquist, and A. Hagfeldt: *J. Phys. Chem. B* **105** (2001) 3350.
- 10) K. Yu, Z. Jin, X. Liu, J. Zhao, and J. Feng: *Appl. Surf. Sci.* **253** (2007) 4072.
- 11) C.-C. Ting, C.-H. Li, C.-Y. Kuo, C.-C. Hsu, H.-C. Wang, and M.-H. Yang: *Thin Solid Films* **518** (2010) 4156.
- 12) S. Yun, J. Lee, J. Yang, and S. Lim: *Physica B* **405** (2010) 413.
- 13) R.-C. Wang, C.-P. Liu, J.-L. Huang, and S.-J. Chen: *Appl. Phys. Lett.* **88** (2006) 023111.
- 14) M. H. Mamat, Z. Khusaimi, M. Z. Musa, M. Z. Sahdan, and M. Rusop: *Mater. Lett.* **64** (2010) 1211.
- 15) M. H. Mamat, M. Z. Sahdan, S. Amizam, H. A. Rafeaie, Z. Khusaimi, and M. Rusop: *J. Ceram. Soc. Jpn.* **117** (2009) 1263.
- 16) K. Govender, D. S. Boyle, P. B. Kenway, and P. O'Brien: *J. Mater. Chem.* **14** (2004) 2575.

- 17) J. Chung, J. Lee, and S. Lim: *Physica B* **405** (2010) 2593.
- 18) H. Zhou, H. Alves, D. M. Hofmann, W. Kriegseis, B. K. Meyer, G. Kaczmarczyk, and A. Hoffmann: *Appl. Phys. Lett.* **80** (2002) 210.
- 19) B. Lo, J.-Y. Chang, A. V. Ghule, S.-H. Tzing, and Y.-C. Ling: *Scr. Mater.* **54** (2006) 411.
- 20) D. Li, Y. H. Leung, A. B. Djuricic, Z. T. Liu, M. H. Xie, S. L. Shi, S. J. Xu, and W. K. Chan: *Appl. Phys. Lett.* **85** (2004) 1601.
- 21) K. H. Tam, C. K. Cheung, Y. H. Leung, A. B. Djuricic, C. C. Ling, C. D. Belling, S. Fung, W. M. Kwok, W. K. Chan, D. L. Phillips, L. Ding, and W. K. Ge: *J. Phys. Chem. B* **110** (2006) 20865.
- 22) C.-Y. Wong, L.-M. Lai, S.-L. Leung, and V. A. L. Roy: *Mater. Sci. Eng. B* **164** (2009) 80.
- 23) C.-C. Lin, H.-P. Chen, H.-C. Liao, and S.-Y. Chen: *Appl. Phys. Lett.* **86** (2005) 183103.
- 24) B. Angadi, H. C. Park, H. W. Choi, J. W. Choi, and W. K. Choi: *J. Phys. D* **40** (2007) 1422.
- 25) B. J. Coppa, C. C. Fulton, S. M. Kiesel, R. F. Davis, C. Pandarinath, J. E. Burnette, R. J. Nemanich, and D. J. Smith: *J. Appl. Phys.* **97** (2005) 103517.
- 26) J. Lee, J. Chung, and S. Lim: *Physica E* **42** (2010) 2143.
- 27) X. Q. Zhao, C. R. Kim, J. Y. Lee, C. M. Shin, J. H. Heo, J. Y. Leem, H. Ryu, J. H. Chang, H. C. Lee, C. S. Son, B. C. Shin, W. J. Lee, W. G. Jung, S. T. Tan, J. L. Zhao, and X. W. Sun: *Appl. Surf. Sci.* **255** (2009) 5861.
- 28) M. Qiu, Z. Ye, J. Lu, H. He, J. Huang, L. Zhu, and B. Zhao: *Appl. Surf. Sci.* **255** (2009) 3972.
- 29) Z. Khusaimi, S. Amizam, M. H. Mamat, M. Z. Sahdan, M. K. Ahmad, N. Abdullah, and M. Rusop: *Synth. React. Inorg. Met.-Org. Nano-Met. Chem.* **40** (2010) 190.
- 30) M. Guo, P. Diao, X. Wang, and S. Cai: *J. Solid State Chem.* **178** (2005) 3210.
- 31) Y. W. Chen, Q. Qiao, Y. C. Liu, and G. L. Yang: *J. Phys. Chem. C* **113** (2009) 7497.
- 32) O. Lupan, L. Chow, G. Chai, B. Roldan, A. Naitabdi, A. Schulte, and H. Heinrich: *Mater. Sci. Eng. B* **145** (2007) 57.
- 33) A. Sugunan, H. C. Warad, M. Boman, and J. Dutta: *J. Sol-Gel Sci. Technol.* **39** (2006) 49.
- 34) R. A. Laudise and A. A. Ballman: *J. Phys. Chem.* **64** (1960) 688.
- 35) R. A. Laudise, E. D. Kolb, and A. J. Caporaso: *J. Am. Ceram. Soc.* **47** (1964) 9.
- 36) X. Tang, E. S. G. Choo, L. Li, J. Ding, and J. Xue: *Chem. Mater.* **22** (2010) 3383.
- 37) G. Niarchos, E. Makarona, and C. Tsamis: *Microsyst. Technol.* **16** (2010) 669.
- 38) C. Chandrinoua, N. Boukosa, K. Giannakopoulou, and A. Lussou: *Superlattices Microstruct.* **42** (2007) 431.
- 39) S. Baruah and J. Dutta: *J. Sol-Gel Sci. Technol.* **50** (2009) 456.
- 40) J. Y. Chen and K. W. Sun: *Sol. Energy Mater. Sol. Cells* **94** (2010) 930.
- 41) K. Yu, Z. Jin, X. Liu, Z. Liu, and Y. Fu: *Mater. Lett.* **61** (2007) 2775.
- 42) T. Hirate, T. Kimpara, S. Nakamura, and T. Satoh: *Superlattices Microstruct.* **42** (2007) 409.